ACS Chemical Neuroscience

pubs.acs.org/chemneuro Research Article

Computational Insights into the Binding of Monolayer-Capped Gold Nanoparticles onto Amyloid-β Fibrils

Francesco Tavanti,* Alfonso Pedone, Maria Cristina Menziani, and Alfredo Alexander-Katz

Cite This: *ACS Chem. Neurosci.* 2020, 11, 3153−3160 Read Online

ACCESS | Metrics & More | Article Recommendations | Supporting Information

ABSTRACT: Amyloids-β (Aβ) fibrils are involved in several neurodegenerative diseases. In this study, atomistic molecular dynamics simulations have been used to investigate how monolayer-protected gold nanoparticles interact with Aβ(1−40) and Aβ(1−42) fibrils. Our results show that small gold nanoparticles bind with the external side of amyloid-β fibrils that is involved in the fibrillation process. The binding affinity, studied for both kinds of fibrils as a function of the monolayer composition and the nanoparticle diameter, is modulated by hydrophobic interactions and ligand monolayer conformation. Our findings thus show that monolayer-protected nanoparticles are good candidates to prevent fibril aggregation and secondary nucleation or to deliver drugs to specific fibril regions.

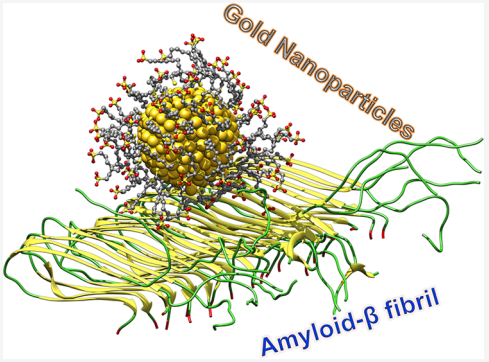

KEYWORDS: *Molecular dynamics simulation, binding affinity, gold nanoparticles, amyloid fibrils, Alzheimer's*

INTRODUCTION

Amyloid fibrils constitute a group of proteins involved in neurodegenerative (typically fatal) diseases such as Alzheimer's (AD), Parkinson's (PD), and Huntington's (HD) disease.[1,2] In particular, β-amyloid peptides ($A\beta_{1-40}$ and $A\beta_{1-42}$) are responsible for fibrous plaque formation in AD,[3] which causes a progressive loss of memory, cognitive deprivation, and death to patients.[4] To date, there are no powerful diagnostic tools for early diagnosis or treatments able to efficiently inhibit the amyloid fibrillation, but this is considered one of the most promising ways to fight AD.[3,5,6]

Amyloid-β fibrils are made by two β-sheets forming a U-shape monomer which is stabilized by a salt bridge between residue D23 and residue K28, which correspond to aspartic acid and lysine, respectively.[7−9] The protofibril is made by parallel β-strands where the two β-sheets, called β-1 and β-2, are perpendicular to the fibril axis, and adjacent monomers are stabilized by hydrogen bonds.[7] It is now recognized that amyloid-β fibrils grow in two distinct ways.[1,10] The addition of A-β monomers to the ends of the fibril along the fibril axis produces fibril elongation, whereas the lateral binding of two fibrils along the fibril axis brings about the formation of the protofilament.[11]

The contact between the two fibrils generally occurs through the β-strands with the β-2 β-sheets exposing the other β-strand to the environment.[7] However, recent studies have shown other possible lateral aggregation processes involving three-folded fibrils[12] which yield several polymorphs, making the understanding of the fibrillation process more complex.[13−15]

Several works have demonstrated that the fibrillation process can be accelerated or retarded by the presence of nanoparticles.[16−18] Recently, Liao et al.[19] studied how 30-nm-diameter negatively charged gold nanoparticles (AuNPs) interact with A-β fibrils finding that AuNPs bind preferentially to mature fibrils; they proposed a mechanism where AuNPs can serve as nanochaperones for the inhibition of Aβ fibrillation. In a recent work, Gao et al.[20] found that 36- and 18-nm-diameter AuNPs covered by L-glutathione accelerate the growth of Aβ fibrils, while 6-nm-diameter AuNPs have the opposite trend, making them good candidates for developing new anti-AD drugs. The same research group interestingly showed how small Au nanoclusters covered with Cys-Arg dipeptides are able to completely dissolve mature fibrils into monomers.[21] Moreover, NPs can act as specific probes for the diagnosis of amyloidosis as recently pointed out by several studies: Cendrowska et al.[22] used 11-mercapto-1-undecanesulfonate (MUS)-coated AuNPs to efficiently assess the morphological polymorphism of different amyloidogenic proteins, such as A-β fibrils and α-synuclein, and other types of Au nanoparticles with mercaptoundecanoic sulfonate as the capping ligand[23] or citrate-capped AuNPs by Elbassal et al.[24] or as shown by Pansieri et al.[25] using functionalized gadolinium

Received: July 31, 2020
Accepted: September 14, 2020
Published: September 14, 2020

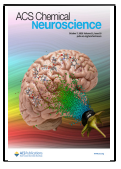

https://dx.doi.org/10.1021/acschemneuro.0c00497
ACS Chem. Neurosci. 2020, 11, 3153−3160

NPs (GdNP) have also been used. Moreover, the recent work of Cendrowska et al.[22] showed that covering the AuNP only with MUS ligands can bind to Aβ fibrils but in a random manner, while the addition of hydrophobic 1-octanethiol (OT) to MUS in a ratio of 4:1 increases the hydrophobic contacts with the fibrils without altering the AuNP solubility.

More broadly, understanding the interaction of AuNPs with biological objects has become of primary importance in nanoscience and in nanotechnological applications.[26−30] AuNPs size and surface composition is a key factor in determining the interaction with proteins[31−36] and with biological membranes,[37−42] but a complete description of these interactions is still missing due to the high number of variables involved. A recent experimental and computational study by Brancolini et al.[43] has provided an explanation of the interaction between 5-nm-diameter citrate-capped AuNPs and the fibrillogenic protein β-2 microglobulin. Their results have suggested that the AuNP-protein interactions and protein orientation upon binding are mainly driven by electrostatic interactions due to the presence of citrates covering the AuNP surface. Moreover, citrate-capped AuNPs do not induce protein fibrillation but could affect His31 amino acid which is involved in the protein destabilization toward an amyloidogenic intermediate.[43] In a recent computational work of Bellucci et al.,[44] it has been shown that a bare Au(111) flat surface can inhibit the fiberlike conformation of an amyloid fibrillar (16−22) peptide. The same authors have demonstrated that the interaction of a single length Aβ_{1-42} peptide with a Au(111) flat surface increases the fibrillar structures due to the high number of contacts that the gold slab flat geometry imposes.[44]

The aim of this study is to elucidate how monolayer-coated AuNPs can act both as markers for amyloid-β fibrils polymorphisms, as recently shown,[22] but also as possible drug carriers to specific fibril regions. For this purpose, we employed that molecular dynamics simulations are the best tools to have an in-depth view at the molecular level of the complex mechanisms that regulates the adsorption of AuNPs over amyloid-β fibrils.

RESULTS AND DISCUSSION

To elucidate the interaction of monolayer-coated AuNPs with both Aβ(1−42) and Aβ(1−40) fibrils, we simulated monolayer-coated AuNPs with a core diameter of 2 and 5 nm interacting with a nonmature protofibril, by means of atomistic molecular dynamics (MD) simulations. Monolayer-coated AuNPs were built according to the previous work of Van Lehn et al.,[38] see Figure 1, changing the monolayer composition and the core diameter, as reported in Methods according to the work of Cendrowska et al.[22] Two sizes of the core AuNP were chosen as 2 and 5 nm in order to have a comparison between different NP sizes. For the 2-nm AuNP, two coatings were studied in order to understand how the coating affects the binding to amyloid fibrils: only MUS and MUS:OT with a ratio of 70:30. As shown in our previous study,[22] these coatings were shown to be highly efficient in labeling the Aβ(1−40) polymorphisms, whereas higher concentrations of OT reduce NP solubility. The Aβ(1−40) protofibril structure is retrieved from the work of Petkova et al.[8] and has been used in our recent studies,[22,45,46] and the Aβ(1−42) protofibril structure is retrieved from the work of Lührs et al.,[7] see Figure 1. The system is placed in a cubic box with the same height of the protofibril, and periodic boundary

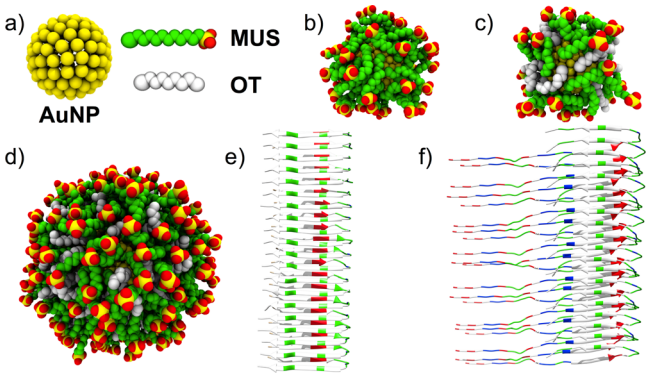

Figure 1. a) Representation of the bare 2-nm AuNP and of its hydrophilic 11-mercapto-1-undecanesulfonate (MUS) and hydrophobic 1-octanethiol (OT) ligands. In panels b) and c) 2-nm-diameter AuNPs are covered with all MUS and 70%MUS-30%OT, respectively, while in panel d) a 5-nm-diameter 70%MUS-30%OT AuNP is shown. MUS ligands are colored green with the heads colored yellow (sulfur) and red (oxygen), while OT ligands are colored white. In panels e) and f) the structures of Aβ(1−42) and Aβ(1−40), side view. Periodic boundary conditions are not shown for clarity. Protofibrils are colored according to amino acid hydrophobicity and charge (hydrophobic in white, hydrophilic in green, positively charged in blue, and negatively charged in red).

conditions are applied allowing the interaction of the fibril endings with their images at the boundaries in order to obtain a continuous indefinitely long protofibril as previously done by Buchete et al.[47]

For each MD run, the protofibril is placed in the center of the simulation box, while one AuNP is randomly displaced, making sure that they are not in contact with each other. The spontaneous binding of many different kinds of monolayer-coated AuNPs to Aβ(1−40) and to Aβ(1−42) fibrils is observed during the simulation runs both by visual inspection and by the number of contacts of the AuNP with the fibrils, as reported in Figure S.3. In the case of the Aβ(1−42) fibril, we found that, whatever coated the 2-nm AuNPs interacts directly with the side of the protofibril in correspondence to the elbow (amino-acid sequence: ^{27}NKGAI^{31}) which links the two β-sheets, and it is characterized by the presence of both hydrophobic and hydrophilic amino acids. At the beginning of the MD simulation, the interaction is given by the contact of ligands covering the AuNP with hydrophilic amino acids located near the head of the beta-1 β-sheet, and then after 20 ns, the AuNP moves toward the region with hydrophobic amino acids closer to the tail of the beta-2 region, see Figure 2a and 2b. This behavior is found for all kinds of 2-nm AuNPs, and we called this binding site "elbow binding". This configuration is characterized by a persistent interaction for the rest of the simulation (as shown in Figure S.3) of the AuNPs with Gly29, Ala30, and Ile31 amino acids, suggesting that this is a possible stable binding site.

In addition, a second binding site (named "β-2 binding") located on the β-2 β-sheet (amino-acid sequence: ^{31}IIGLMV-GGVVI^{41}) is observed, see Figure 2c and 2d. In this case, the AuNPs interact at first with the region between the elbow and the β-2 β-sheet, and after 10 ns, the AuNP moves along the β-sheet. Amino acids involved in the binding have their side chain pointed outward, and they are Ile31, Gly33, Met35, Gly37, Val39, and Ile41. Also, in this case, all AuNPs remain bound to the β-sheet for the remainder of the simulation time.

https://dx.doi.org/10.1021/acschemneuro.0c00497
ACS Chem. Neurosci. 2020, 11, 3153−3160

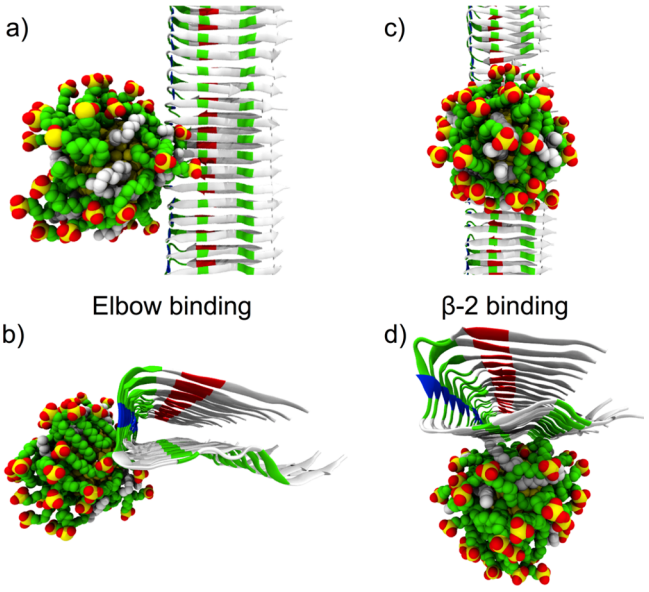

Figure 2. In a) and b) the elbow binding of the 2-nm 70%MUS-30% OT AuNP on the protofibril, while in c) and d) the β-2 binding as seen from the top and front of the fibril. Only the secondary structure of the protofibril is represented for clarity. Amino acids are colored according to their hydrophobicity and their net charge: hydrophobic amino acids are represented in white, hydrophilic amino acids are represented in green, positively charged amino acids are represented in blue, and negatively charged amino acids are represented in red. Heads of MUS ligands are colored according to the atom type: sulfur in yellow and oxygen in red.

Both binding modalities are supported by the recent results of Cendrowska et al.[22] where they showed that coated AuNPs can be used to label the edge of different amyloidogenic proteins, such as Aβ(1−40) fibrils.

The 5-nm-diameter AuNP is found to bind with the Aβ(1−42) protofibril over the 100 ns simulations only in the elbow region, while it is never found to interact with β-sheet regions suggesting the presence of a possible potential barrier that could, in principle, be overcome by using longer time scales that are not affordable with full atomistic simulations.

For simulations of Aβ(1−40), the 2- and 5-nm AuNPs interact with the beta-1 region of the protofibril ("β-1 binding"), making stable contacts with the amino acids from His14 to Phe20. During the simulations involving the 70/30 2-nm AuNP, we observed that amino acids in the Aβ(1−40) tails interact with the AuNP before its binding to the fibril, see Figure 3a. In this case, up to 4 tails grab the AuNP especially through Ala2 and Phe4 amino acids establishing hydrophobic interactions. In the simulation with the 2-nm allMUS AuNP, an Aβ(1−40) tail seems to mediate the interaction with the AuNP driving the binding to the beta-1 region. The first interaction happens through a MUS ligand and residues Arg5 and His6 that grab the tail of the MUS ligand, see Figure 3b, and then the AuNP is close enough to the protofibril to interact with the beta-1 region to form a stable contact.

The 5-nm AuNP spontaneously binds to the β-1 region where the adsorption is mediated by a tail that makes the first binding as for the 2-nm AuNP case, but it is not able to grab the AuNP due to its size. In this case, the AuNP adsorbs over the fibril, but coated ligands cannot be accommodated into the protofibril shape because they are closely packed together.

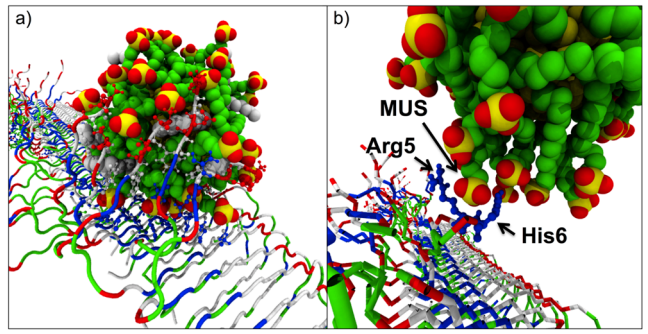

Figure 3. In panel a) a snapshot of the simulation of the 70/30 AuNP bound to the beta-1 region of the Aβ(1−40) protofibril grabbed by 5 tails. In panel b) are shown an arginine (R5) and a histidine (H6) grabbing the head of a MUS ligand in the early steps of the binding of all the MUS AuNP with the Aβ(1−40) fibril. Amino acids are colored according to their hydrophobicity and their net charge: hydrophobic amino acids are represented in white, hydrophilic amino acids are represented in green, positively charged amino acids are represented in blue, and negatively charged amino acids are represented in red. Heads of MUS ligands are colored according to the atom type: sulfur in yellow and oxygen in red.

In all simulations, the protofibril secondary structure shows no changes in the β-sheets and in the elbow regions. Small conformational changes are found only in the highly mobile tails close to the N-terminal region, as recently found.[45]

Computational and experimental studies on the Aβ fibrils have highlighted the presence of several binding sites mainly located in proximity to the two β-sheets comprising amino acids Leu17 - Ala21 and Gly33 - Val40.[48,49] Chalifour et al.[50] used circular dichroism and electron microscopy to show that the stretch of residues 16−20 on Aβ(1−40) fibrils acts as a possible receptor for peptides to prevent amyloid fibrillation. The (^{16}KLVFFA^{21}) motif has also been studied as possible binding sites for antifibrillation curcumin-like drugs by using molecular docking and MD simulations[51] and by UV−visible spectroscopy and fluorescence quenching studies.[52] The results of molecular docking by Chen et al.[53] have shown three main interaction sites for the binding of peptides to Aβ(1−40): they comprise amino acids 28−32 and amino acids 11−19 and 34−40.

The binding site found in the present work for Aβ(1−40) spans His14 to Phe20 (^{14}HQKLVFFA^{21}) in agreement with the predicted binding site (^{16}KLVFFA^{21}) for drugs and peptides reported in the literature by several studies.[51,52,54,55]

The His14 to Phe20 region, characterized by a β-sheet folding, is thought to be responsible for the secondary nucleation process, i.e., the lateral aggregation of amyloid monomers onto preformed fibrils that bring about the formation of mature fibrils.[56] The AuNPs interacting with the Aβ(1−40) in this specific region can act as a spacer disturbing the binding of additional fibrils and, in principle, can inhibit or retard the secondary nucleation process.

Table 1 lists a number of descriptors, computed on 100 ns simulation runs after binding, considered to characterize the interactions between the AuNPs and the Aβ fibrils.

Analysis of the data values shows that

1) In the case of Aβ(1−42), the number of contacts between the AuNP monolayer and the protofibril is higher in the β-2 binding for all AuNP compositions with respect to the elbow binding.

https://dx.doi.org/10.1021/acschemneuro.0c00497
ACS Chem. Neurosci. 2020, 11, 3153−3160

Table 1. Number of Contacts, RMSD of the Fibril after the Binding, and DG_{phobic} Calculated for the Different AuNP Monolayer Compositions and Diameters Interacting with the Aβ(1−42) and with the Aβ(1−40)

	binding site	2 nm[a] 70/30[b]	2 nm[a] 100/0[b]	5 nm[a] 70/30[b]
		Aβ(1−42)		
no. of contacts	elbow	140 ± 10	135 ± 10	145 ± 15
	β-2	180 ± 15	180 ± 16	195 ± 25
RMSD (nm)	elbow	0.48 ± 0.02	0.54 ± 0.04	0.32 ± 0.02
	β-2	0.42 ± 0.03	0.46 ± 0.03	0.33 ± 0.01
DG_{phobic} (kcal/mol)	elbow	−128 ± 47	−169 ± 47	−99 ± 94
	β-2	−139 ± 52	−184 ± 52	−174 ± 94
		Aβ(1−40)		
no. of contacts	β-1	220 ± 15	180 ± 20	120 ± 15
RMSD (nm)	β-1	0.49 ± 0.02	0.54 ± 0.03	0.34 ± 0.01
DG_{phobic} (kcal/mol)	β-1	−197 ± 56	−179 ± 47	−202 ± 80

[a]AuNP diameter. [b]Monolayer composition.

2) All the AuNPs establish a similar number of contacts with the β-2 region of the Aβ(1−42) protofibril, whereas in the case of the Aβ(1−40) protofibril, a higher number of contacts is observed for the 70/30 AuNP (2 nm) due to the interaction with the protofibril's tails.
3) Overall, the stability of the binding, as highlighted by the RMSD, seems to be slightly lower for the 2-nm AuNPs studied with respect to the 5-nm AuNP.
4) The estimation of the hydrophobic component of the DG energy (DG_{phobic}), see the SI, shows that the β-2 binding mode is always more stable than the elbow one, and the stability increases with the number of MUS ligands on the monolayer. The DG_{phobic} of the β-2 binding mode of the 5-nm AuNP to the Aβ(1−42) protofibril is double with respect to the elbow binding mode, in agreement with our observation made by the visual analysis of the trajectory that the ligands do not fit the protofibril structure.

To gain deeper insight into the β-sheet and elbow binding sites in the fibrils, we computed the potential of mean force (PMF) using the Umbrella sampling methodology, as reported in the SI. We found that the binding energies are fibril dependent and are modulated by both the coating chemistry and the size of the AuNPs. For the Aβ(1−42) fibril, the β-2 binding energies are about 10 kcal/mol more stable than the elbow binding energies for the 2-nm AuNPs, see Table 2, whereas the binding energies for the 5-nm AuNP are similar in both regions. However, a potential barrier of 3.5 kcal/mol is observed for the binding of the 5-nm AUNP to the β-2 region, as reported in Table 2. This barrier is due to the presence of water molecules located in the cavity of the β-2 region that screen the interactions between the 5-nm AuNP and this particular portion of the fibril, preventing spontaneous binding, as shown in Figure S.4. In this case, ligands trap water molecules in the channel given by I31 to G37 due to the bigger size of the AuNP, while the 2-nm AuNPs are sharper and can easily displace water molecules. Values of the PMF for the Aβ(1−40) protofibril show that the allMUS 2-nm AuNP establishes more stable interactions than the other kind of AuNPs bound to the β-1, with energy values similar to those obtained for the β-2 binding in the Aβ(1−42). On the contrary, the 70/30 2-nm AuNP establishes most stable interactions with Aβ(1−40). This difference could be explained by the differences in the amino-acid composition of the two β-sheets of the two fibrils: in the Aβ(1−40), the β1 given by the sequence ^{15}QKLVFFAEDV^{24}, which contains charged amino acids, and the β1 given by the sequence ^{30}AIIGLMVGGVV^{40}, which is mainly hydrophobic. It is important to note that the total free energy of binding is much lower in magnitude compared to DG_{phobic}, which implies that upon binding there is a strong entropic penalty presumably stemming from the ligand rearrangements. To put it in perspective, these binding free energies are much smaller than those for the same nanoparticles and lipid bilayers.[38] Moreover, the forces calculated for each nanoparticle in the case of Aβ(1−42) fibrils decrease with the binding energy, while an opposite trend is observed for Aβ(1−40) fibrils where higher energies are related to low forces, as reported in Figure 4 and in Table 2.

Table 2. Binding Energies, Potential Barriers, and Forces for Different Monolayer Compositions for the 2- and 5-nm-Diameter AuNPs Expressed in kcal/mol and Centers of Mass (CoM) Distances Expressed in nm[a]

		binding site	2 nm 70/30	2 nm 100/0	5 nm 70/30
Aβ(1−42)	elbow	binding energy	−55	−45	−23
		CoM distance	2.25	2.25	4.24
		potential barrier			
		force (kJ/mol)	218.86	239.73	96.86
	β-2	binding energy	−65	−54	−29
		CoM distance	3.15	3.15	4.94
		potential barrier			3.5
		force (kJ/mol)	282.26	257.52	239.03
Aβ(1−40)	β-1	binding energy	−24	−51	−38
		CoM distance	3.55	3.50	4.65
		potential barrier			
		force (kJ/mol)	219.7	170.43	184.99

[a]Binding energy values are computed at the distance between the CoM of the AuNP and the protofibril reported below. The force values correspond to the maximum value of the derivative of the Morse potential fitted over the binding energy values reported in the SI.

In order to assess the average number of AuNPs able to bind to a fibril per unit length, we have estimated the closest distance at which two AuNPs can bind on the same binding site by computing the distance, d_{CoM}, at which the electrostatic repulsion, $E_{repulsion}(d_{CoM})$, is equal to the absolute value of the binding energy, $E_{binding}$, on that site, as reported in eq 1. Details of the computations are reported in the SI.

$$E_{repulsion}(d_{CoM}) = |E_{binding}| \quad (1)$$

The minimum distance is mainly governed by the net charge of the AuNP. Thus, the 70/30 2-nm AuNP can reach a shorter separation with respect to 5-nm AuNPs that has a higher net charge due to the increased number of MUS ligands, see Table 3. For the Aβ(1−40), the 2-nm AuNPs can reach the same

https://dx.doi.org/10.1021/acschemneuro.0c00497
ACS Chem. Neurosci. 2020, 11, 3153−3160

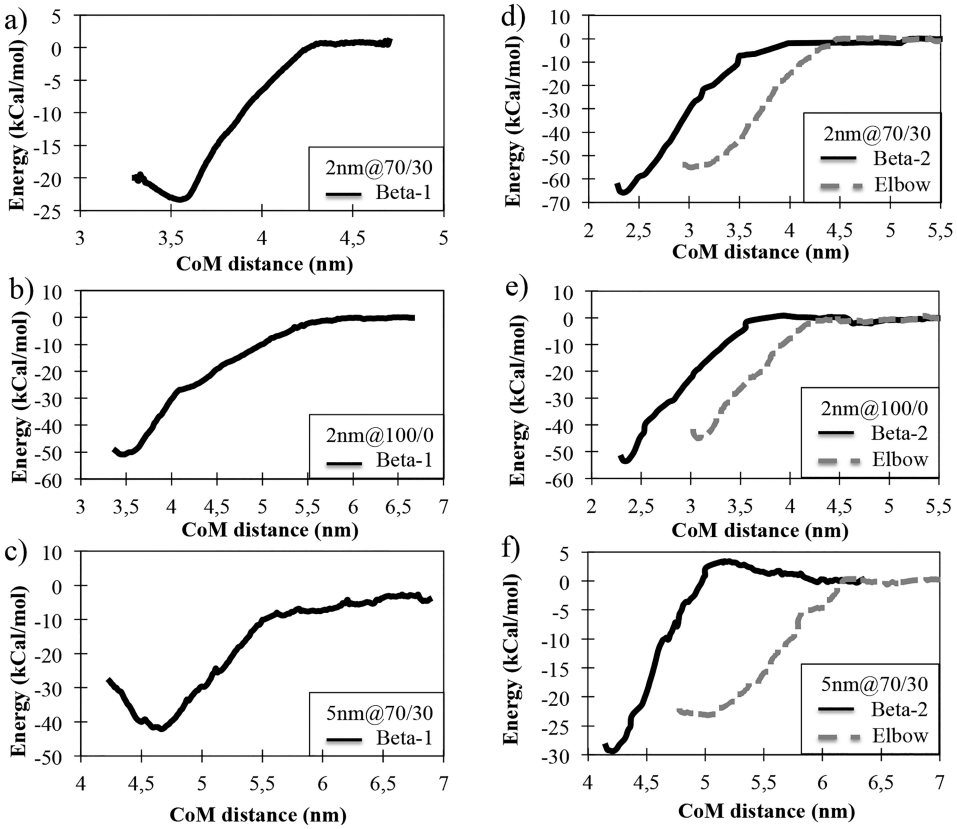

Figure 4. Potential of mean force expressed in kcal/mol versus the distance between the centers of mass of the AuNP and the fibril. In panels a)−c) is shown the PMF for Aβ(1−40) fibrils, while in panels d)−f) the black continuous line represents the front binding, and the gray dashed line represents the side binding for Aβ(1−42) fibrils.

Table 3. Minimum Separation Distance, d_{CoM} (in nm), between Two AuNPs When the Electrostatic Repulsion Is Equal to the Absolute Value of the Binding Energy

	binding site	70/30 2 nm	100/0 2 nm	70/30 5 nm
Aβ(1−42)	elbow	4.59	4.83	5.86
	β-2	4.54	4.77	5.79
Aβ(1−40)	β-1	4.80	4.79	5.71

minimum distance because the repulsive charge effect is balanced by the binding energy difference. The 2-nm 70/30 NPs bound to the Aβ(1−42) can reach the smaller distances due to the high binding energy. These calculations do not take into account the possible effects at the short-range scale that can affect the AuNPs aggregation as reported in a previous computational work by Van Lehn et al.[57]

In summary, we have shown that small monolayer-protected AuNPs are able to bind to both Aβ(1−40) and to Aβ(1−42) without altering the protein secondary structures. For all three kinds of AuNPs considered, the binding happens on the external protofibril regions characterized by the presence of two β-sheets made by hydrophobic amino acids and in correspondence to residues that are responsible for fibril aggregation. Importantly, the binding of AuNPs with the Aβ(1−40) is mediated by the protofibril tails that drive the interaction to the β-1 β-sheet. These results clearly show the potential of gold nanoparticles to both inhibit the fibrillation process, in particular the 2-nm MUS:OT 70:30 coated AuNPs efficiently target the Aβ(1−42) fibrils, and to act as possible carriers for drugs to fight Alzheimer's disease.

METHODS

Molecular Dynamics Simulations. Molecular dynamics simulations were performed to simulate the interaction of a gold NP with the amyloid-β (Aβ) protofibril in physiological conditions. Aβ(1−40) and Aβ(1−42) have a similar secondary structure, and they differ in their amino acid sequence only in the last two residues (Aβ(1−40) FASTA sequence: DAEFRHDSGYEVHHQKLVFFAEDVGSNKGAIIGLMVGGVVIA;[8] Aβ(1−42) FASTA sequence: DAEFRHDSGYEVHHQKLVFFAEDVGSNKGAIIGLMVGGVV[7]).

The Aβ(1−40) protofibril structure was obtained from the previous work of Petkova et al.[8] (PDB ID: 2LMN), while the Aβ(1−42) protofibril structure was obtained from the work of Lührs et al.[7] (PDB ID: 2BEG). Both structures were already used in previous computational studies with good results.[58−60] The Aβ(1−42) and the Aβ(1−40) fibrils were built replicating the reference structure 4 times along its principal axis obtaining a continuous structure 9.805 nm long made by 20 monomers. An acetyl group was added to cap each N-terminus chain in order to mimic missing amino acids forming the peptide, whereas deprotonated C-terminus were used, according to the work of Lemkul et al.[59] The first 8 missing amino acids of Aβ(1−40) were inserted using the Molefacture plugin in the VMD package[61] as random coils as predicted by both the Jpred web server[62] and by the Modeler package[63] for protein secondary structure assignments, as previously done.[45,46] The same procedure is not suitable for the Aβ(1−42) structure due to the high number of missing amino acids and to the consequent inability to accurately simulate the fibril.

The protofibril was placed in an orthorhombic box with the same height of the fibril. The protofibril in the box interacts with its images at the top and at the bottom of the box forming a continuous structure along the z direction.

The 2- and 5-nm-diameter AuNPs were built according to the work of Van Lehn et al.[64] The gold core is hollow, and missing gold atoms

https://dx.doi.org/10.1021/acschemneuro.0c00497
ACS Chem. Neurosci. 2020, 11, 3153−3160

masses are redistributed uniformly to shell atoms. Hydrophilic 11-mercapto-1-undecanesulfonate (MUS) and hydrophobic 1-octanethiol (OT) ligands were grafted to the AuNP surface via their sulfur atoms. Van Lehn et al.[64] showed that AuNP surface structural characteristics are not affected by different ligand morphologies but only by the NP size and ligands relative lengths. In this study, we used a random morphology. Three 2-nm-diameter AuNPs were coated with two different ligand compositions: a) 70%MUS-30%OT and b) 100%MUS-0%OT. In the text of the article, these AuNPs are labeled with their composition (70/30 and allMUS) for brevity. The 5-nm-diameter AuNP is covered by 70%MUS-30%OT. The overall charge of the AuNP is given by the number of MUS ligands forming the protecting monolayer.

For all simulations, the GROMOS 54a7 united atom force field[65] modified by Van Lehn et al.[64] to include potentials for ligands was used to model both the protofibril and the AuNP.[64−66] Simple point charge (SPC) water[67] was added, and water molecules inside the hollow gold core were removed. A salt concentration of 150 mM was used, and the system was neutralized with the use of counterions.

Electrostatics interactions[68,69] were computed by the particle-mesh Ewald (PME) algorithm, using a fourth-order cubic interpolation, a grid spacing of 0.16 nm, and a real-space cutoff of 1 nm, as described by Van Lehn et al.[64] Both van der Waals and neighbor list cutoffs for short-range interactions were set to 1.0 nm. The temperature was kept constant at 310 K, and the pressure was set to 1 bar in order to mimic physiological conditions. The temperature was controlled using a velocity-rescaling thermostat with a coupling time of 0.1 ps. During the equilibration run, the pressure was controlled by the Berendsen barostat, while during the production run, the pressure was controlled by the Parrinello-Rhaman barostat with a coupling time of 2 ps and an isothermal compressibility of 4.5×10^{-5} bar^{-1}. All simulations were 100 ns long, and the time step used was 2.0 fs.

For each simulation, the protofibril was placed at the center of the simulation box with one AuNP randomly positioned making sure that they are not in contact. The number of water molecules in each simulation is slightly different due to the AuNP embedding process. For each different AuNP composition and diameter, three simulations of 100 ns with different starting configurations were performed. All simulations and data analysis were performed using the Gromacs-5.0.4 package.[70]

Data Analysis. Data analysis was performed using the Gromacs package.[70] The root mean square displacement (RMSD) was calculated for the coated AuNP after the binding to the fibril. The RMSD calculations give a measure of the stability of the AuNP after the binding.

The change in the free energy (DG_{phobic}) was obtained explicitly as the DSASA multiplied by the constant γ which is the parameter controlling the magnitude of the hydrophobic driving force. The value of γ is 4.7 kcal/mol according to previous works of Van Lehn et al.[71,72] and of Sharp et al.[73] The SASA is a measure of the hydrophobic material exposed to the solvent at each simulation time step and was calculated by the Shrake-Rupley "rolling ball" algorithm[74] by the use of 100 uniformly distributed mesh points per hydrophobic bead and a 0.14-nm probe size to reproduce water solvation.

The number of contacts between the polymer monolayer and the fibrils during the simulation time is given by the number of atoms of the monolayer that have a distance less than 0.5 nm from any one atom of the fibril.

All average values and errors have been computed by averaging data through the simulation length using the Gromacs tools.[70]

■ ASSOCIATED CONTENT

Supporting Information

The Supporting Information is available free of charge at https://pubs.acs.org/doi/10.1021/acschemneuro.0c00497.

Simulation details, potential of mean force calculation, secondary structure assignment, and electrostatic repulsion expression (PDF)

■ AUTHOR INFORMATION

Corresponding Author

Francesco Tavanti − *Department of Chemical and Geological Sciences, University of Modena and Reggio Emilia, I-41125 Modena, Italy; CNR-NANO Istituto Nanoscienze, I-41125 Modena, Italy;* orcid.org/0000-0002-0594-5308; Email: francesco.tavanti@nano.cnr.it

Authors

Alfonso Pedone − *Department of Chemical and Geological Sciences, University of Modena and Reggio Emilia, I-41125 Modena, Italy;* orcid.org/0000-0003-3772-7222

Maria Cristina Menziani − *Department of Chemical and Geological Sciences, University of Modena and Reggio Emilia, I-41125 Modena, Italy;* orcid.org/0000-0003-3428-5297

Alfredo Alexander-Katz − *Department of Materials Science and Engineering, Massachusetts Institute of Technology, Cambridge, Massachusetts 02142, United States*

Complete contact information is available at: https://pubs.acs.org/10.1021/acschemneuro.0c00497

Author Contributions

A.A.-K. designed the research and models. F.T. performed the simulations and data analysis. A.A.-K. and F.T. discussed the results and interpretation. The manuscript was written through contributions of all authors. All authors have given approval to the final version of the manuscript.

Notes

The authors declare no competing financial interest.

■ ACKNOWLEDGMENTS

We are grateful to Francesco Stellacci and Paulo Henrique Jacob Silva for pointing out this system to one of us (A.A.-K.), as well as for many insightful discussions. This work was supported by the Italian Ministero dell'Istruzione, dell'Università e della Ricerca (MIUR) through the "Programma di ricerca di rilevante interesse nazionale" (PRIN) Grant 2010C4R8M8_002 entitled "Nanoscale Functional Organization of (bio)Molecules and Hybrids for targeted Application in Sensing, Medicine and Biotechnology". F.T. acknowledges the grant "FAR Junior 2018: Computer-aided Rational Design of Functionalized Gold Nanoparticles as Inhibitors of Amyloid-β Oligomerization for Alzheimer's Disease Treatment" from the University of Modena and Reggio Emilia. We acknowledge the CINECA Supercomputing Centre (Italy) by the HPC projects ISCRA-C HP10C4CSIH and HP10CCB4UL for computational resources.

■ REFERENCES

(1) Tycko, R. (2006) Molecular Structure of Amyloid Fibrils: Insights from Solid-State NMR. *Q. Rev. Biophys. 39* (01), 1−55.

(2) Selkoe, D. J. (2003) Folding Proteins in Fatal Ways. *Nature 426* (6968), 900−904.

(3) Roychaudhuri, R., Yang, M., Hoshi, M. M., and Teplow, D. B. (2009) Amyloid β-Protein Assembly and Alzheimer Disease. *J. Biol. Chem. 284* (8), 4749−4753.

(4) Tanzi, R. E., and Bertram, L. (2005) Twenty Years of the Alzheimer's Disease Amyloid Hypothesis: A Genetic Perspective. *Cell 120* (4), 545−555.

(5) Landau, M., Sawaya, M. R., Faull, K. F., Laganowsky, A., Jiang, L., Sievers, S. A., Liu, J., Barrio, J. R., and Eisenberg, D. (2011) Towards a Pharmacophore for Amyloid. *PLoS Biol. 9* (6), No. e1001080.

(6) Stains, C. I., Mondal, K., and Ghosh, I. (2007) Molecules That Target Beta-Amyloid. *ChemMedChem 2* (12), 1674−1692.
(7) Lührs, T., Ritter, C., Adrian, M., Riek-Loher, D., Bohrmann, B., Döbeli, H., Schubert, D., and Riek, R. (2005) 3D Structure of Alzheimer's Amyloid-β(1−42) Fibrils. *Proc. Natl. Acad. Sci. U. S. A. 102* (48), 17342−17347.
(8) Petkova, A. T., Yau, W.-M., and Tycko, R. (2006) Experimental Constraints on Quaternary Structure in Alzheimer's β-Amyloid Fibrils†. *Biochemistry 45* (2), 498−512.
(9) Tavanti, F., Pedone, A., and Menziani, M. C. (2020) Insights into the Effect of Curcumin and (−)-Epigallocatechin-3-Gallate on the Aggregation of Aβ(1−40) Monomers by Means of Molecular Dynamics. *Int. J. Mol. Sci. 21*, 5462.
(10) Tycko, R. (2015) Amyloid Polymorphism: Structural Basis and Neurobiological Relevance. *Neuron 86* (3), 632−645.
(11) Stroud, J. C., Liu, C., Teng, P. K., and Eisenberg, D. (2012) Toxic Fibrillar Oligomers of Amyloid-β Have Cross-β Structure. *Proc. Natl. Acad. Sci. U. S. A. 109* (20), 7717−7722.
(12) Paravastu, A. K., Leapman, R. D., Yau, W.-M., and Tycko, R. (2008) Molecular Structural Basis for Polymorphism in Alzheimer's β-Amyloid Fibrils. *Proc. Natl. Acad. Sci. U. S. A. 105* (47), 18349−18354.
(13) Riek, R., Güntert, P., Döbeli, H., Wipf, B., and Wüthrich, K. (2001) NMR Studies in Aqueous Solution Fail to Identify Significant Conformational Differences between the Monomeric Forms of Two Alzheimer Peptides with Widely Different Plaque-Competence, Aβ(1−40)Ox and Aβ(1−42)Ox. *Eur. J. Biochem. 268* (22), 5930−5936.
(14) Meinhardt, J., Sachse, C., Hortschansky, P., Grigorieff, N., and Fändrich, M. (2009) Aβ(1−40) Fibril Polymorphism Implies Diverse Interaction Patterns in Amyloid Fibrils. *J. Mol. Biol. 386* (3), 869−877.
(15) Sachse, C., Xu, C., Wieligmann, K., Diekmann, S., Grigorieff, N., and Fändrich, M. (2006) Quaternary Structure of a Mature Amyloid Fibril from Alzheimer's Aβ(1−40) Peptide. *J. Mol. Biol. 362* (2), 347−354.
(16) Solin, N. (2013) Amyloid-like Fibrils Labeled with Magnetic Nanoparticles. *Biomol. Concepts 4* (4), 425−432.
(17) Majorosova, J., Petrenko, V. I., Siposova, K., Timko, M., Tomasovicova, N., Garamus, V. M., Koralewski, M., Avdeev, M. V., Leszczynski, B., Jurga, S., Gazova, Z., Hayryan, S., Hu, C.-K., and Kopcansky, P. (2016) On the Adsorption of Magnetite Nanoparticles on Lysozyme Amyloid Fibrils. *Colloids Surf., B 146*, 794−800.
(18) Palmal, S., Jana, N. R., and Jana, N. R. (2014) Inhibition of Amyloid Fibril Growth by Nanoparticle Coated with Histidine-Based Polymer. *J. Phys. Chem. C 118* (37), 21630−21638.
(19) Liao, Y.-H., Chang, Y.-J., Yoshiike, Y., Chang, Y.-C., and Chen, Y.-R. (2012) Negatively Charged Gold Nanoparticles Inhibit Alzheimer's Amyloid-β Fibrillization, Induce Fibril Dissociation, and Mitigate Neurotoxicity. *Small 8* (23), 3631−3639.
(20) Gao, G., Zhang, M., Gong, D., Chen, R., Hu, X., and Sun, T. (2017) The Size-Effect of Gold Nanoparticles and Nanoclusters in the Inhibition of Amyloid-β Fibrillation. *Nanoscale 9* (12), 4107−4113.
(21) Zhang, W., Gao, G., Ma, Z., Luo, Z., He, M., and Sun, T. (2020) Au23(CR)14 Nanocluster Restores Fibril Aβ's Unfolded State with Abolished Cytotoxicity and Dissolves Endogenous Aβ Plaques. *Natl. Sci. Rev. 7* (4), 763−774.
(22) Cendrowska, U., Silva, P. J., Ait-Bouziad, N., Müller, M., Guven, Z. P., Vieweg, S., Chiki, A., Radamaker, L., Kumar, S. T., Fändrich, M., Tavanti, F., Menziani, M. C., Alexander-Katz, A., Stellacci, F., and Lashuel, H. A. (2020) Unraveling the Complexity of Amyloid Polymorphism Using Gold Nanoparticles and Cryo-EM. *Proc. Natl. Acad. Sci. U. S. A. 117*, 6866.
(23) Silva, P. H. J. (2016) *Discriminative Adsorption of Amphiphilic Monolayer Protected Gold Nanoparticles on Amyloid Fibers*. PhD Thesis, EPFL, Switzerland, DOI: 10.5075/epfl-thesis-7037.
(24) Elbassal, E. A., Morris, C., Kent, T. W., Lantz, R., Ojha, B., Wojcikiewicz, E. P., and Du, D. (2017) Gold Nanoparticles as a Probe for Amyloid-β Oligomer and Amyloid Formation. *J. Phys. Chem. C 121* (36), 20007−20015.
(25) Pansieri, J., Plissonneau, M., Stransky-Heilkron, N., Dumoulin, M., Heinrich-Balard, L., Rivory, P., Morfin, J.-F., Toth, E., Saraiva, M. J., Allémann, E., Tillement, O., Forge, V., Lux, F., and Marquette, C. (2017) Multimodal Imaging Gd-Nanoparticles Functionalized with Pittsburgh Compound B or a Nanobody for Amyloid Plaques Targeting. *Nanomedicine 12* (14), 1675−1687.
(26) Ghosh, P., Han, G., De, M., Kim, C. K., and Rotello, V. M. (2008) Gold Nanoparticles in Delivery Applications. *Adv. Drug Delivery Rev. 60* (11), 1307−1315.
(27) Lundqvist, M., Stigler, J., Elia, G., Lynch, I., Cedervall, T., and Dawson, K. A. (2008) Nanoparticle Size and Surface Properties Determine the Protein Corona with Possible Implications for Biological Impacts. *Proc. Natl. Acad. Sci. U. S. A. 105* (38), 14265−14270.
(28) Lacerda, S. H. D. P., Park, J. J., Meuse, C., Pristinski, D., Becker, M. L., Karim, A., and Douglas, J. F. (2010) Interaction of Gold Nanoparticles with Common Human Blood Proteins. *ACS Nano 4* (1), 365−379.
(29) Sardar, R., Funston, A. M., Mulvaney, P., and Murray, R. W. (2009) Gold Nanoparticles: Past, Present, and Future. *Langmuir 25* (24), 13840−13851.
(30) Doane, T. L., and Burda, C. (2012) The Unique Role of Nanoparticles in Nanomedicine: Imaging, Drug Delivery and Therapy. *Chem. Soc. Rev. 41* (7), 2885−2911.
(31) Tavanti, F., Pedone, A., and Menziani, M. C. (2015) A Closer Look into the Ubiquitin Corona on Gold Nanoparticles by Computational Studies. *New J. Chem. 39* (4), 2474−2482.
(32) Brancolini, G., Kokh, D. B., Calzolai, L., Wade, R. C., and Corni, S. (2012) Docking of Ubiquitin to Gold Nanoparticles. *ACS Nano 6* (11), 9863−9878.
(33) Tavanti, F., Pedone, A., and Menziani, M. C. (2015) Competitive Binding of Proteins to Gold Nanoparticles Disclosed by Molecular Dynamics Simulations. *J. Phys. Chem. C 119* (38), 22172−22180.
(34) Deyev, S., Proshkina, G., Ryabova, A., Tavanti, F., Menziani, M. C., Eidelshtein, G., Avishai, G., and Kotlyar, A. (2017) Synthesis, Characterization, and Selective Delivery of DARPin−Gold Nanoparticle Conjugates to Cancer Cells. *Bioconjugate Chem. 28* (10), 2569−2574.
(35) Matteini, P., Cottat, M., Tavanti, F., Panfilova, E., Scuderi, M., Nicotra, G., Menziani, M. C., Khlebtsov, N., de Angelis, M., and Pini, R. (2017) Site-Selective Surface-Enhanced Raman Detection of Proteins. *ACS Nano 11* (1), 918−926.
(36) Tavanti, F., Pedone, A., Matteini, P., and Menziani, M. C. (2017) Computational Insight into the Interaction of Cytochrome C with Wet and PVP-Coated Ag Surfaces. *J. Phys. Chem. B 121* (41), 9532−9540.
(37) Leroueil, P. R., Hong, S., Mecke, A., Baker, J. R., Orr, B. G., and Banaszak Holl, M. M. (2007) Nanoparticle Interaction with Biological Membranes. *Acc. Chem. Res. 40* (5), 335−342.
(38) Van Lehn, R. C., Atukorale, P. U., Carney, R. P., Yang, Y.-S., Stellacci, F., Irvine, D. J., and Alexander-Katz, A. (2013) Effect of Particle Diameter and Surface Composition on the Spontaneous Fusion of Monolayer-Protected Gold Nanoparticles with Lipid Bilayers. *Nano Lett. 13* (9), 4060−4067.
(39) Van Lehn, R. C., Ricci, M., Silva, P. H. J., Andreozzi, P., Reguera, J., Voïtchovsky, K., Stellacci, F., and Alexander-Katz, A. (2014) Lipid Tail Protrusions Mediate the Insertion of Nanoparticles into Model Cell Membranes. *Nat. Commun. 5*, 4482.
(40) Lin, J., Dargazany, R., and Alexander-Katz, A. (2017) Lipid Flip-Flop and Pore Nucleation on Zwitterionic Bilayers Are Asymmetric under Ionic Imbalance. *Small 13* (22), 1603708.
(41) Simonelli, F., Bochicchio, D., Ferrando, R., and Rossi, G. (2015) Monolayer-Protected Anionic Au Nanoparticles Walk into Lipid Membranes Step by Step. *J. Phys. Chem. Lett. 6* (16), 3175−3179.

(42) Lin, J., and Alexander-Katz, A. (2013) Cell Membranes Open "Doors" for Cationic Nanoparticles/Biomolecules: Insights into Uptake Kinetics. *ACS Nano* 7 (12), 10799−10808.
(43) Brancolini, G., Corazza, A., Vuano, M., Fogolari, F., Mimmi, M. C., Bellotti, V., Stoppini, M., Corni, S., and Esposito, G. (2015) Probing the Influence of Citrate-Capped Gold Nanoparticles on an Amyloidogenic Protein. *ACS Nano* 9 (3), 2600−2613.
(44) Bellucci, L., Ardèvol, A., Parrinello, M., Lutz, H., Lu, H., Weidner, T., and Corni, S. (2016) The Interaction with Gold Suppresses Fiber-like Conformations of the Amyloid β (16−22) Peptide. *Nanoscale* 8 (16), 8737−8748.
(45) Tavanti, F., Pedone, A., and Menziani, M. C. (2018) Computational Insight into the Effect of Natural Compounds on the Destabilization of Preformed Amyloid-β(1−40) Fibrils. *Molecules* 23 (6), 1320.
(46) Orteca, G., Tavanti, F., Bednarikova, Z., Gazova, Z., Rigillo, G., Imbriano, C., Basile, V., Asti, M., Rigamonti, L., Saladini, M., Ferrari, E., and Menziani, M. C. (2018) Curcumin Derivatives and Aβ-Fibrillar Aggregates: An Interactions' Study for Diagnostic/Therapeutic Purposes in Neurodegenerative Diseases. *Bioorg. Med. Chem.* 26 (14), 4288−4300.
(47) Buchete, N.-V., Tycko, R., and Hummer, G. (2005) Molecular Dynamics Simulations of Alzheimer's β-Amyloid Protofilaments. *J. Mol. Biol.* 353 (4), 804−821.
(48) Kundaikar, H. S., and Degani, M. S. (2015) Insights into the Interaction Mechanism of Ligands with Aβ42 Based on Molecular Dynamics Simulations and Mechanics: Implications of Role of Common Binding Site in Drug Design for Alzheimer's Disease. *Chem. Biol. Drug Des.* 86 (4), 805−812.
(49) Sablón-Carrazana, M., Fernández, I., Bencomo, A., Lara-Martínez, R., Rivera-Marrero, S., Domínguez, G., Pérez-Perera, R., Jiménez-García, L. F., Altamirano-Bustamante, N. F., Diaz-Delgado, M., Vedrenne, F., Rivillas-Acevedo, L., Pasten-Hidalgo, K., Segura-Valdez, M. de L., Islas-Andrade, S., Garrido-Magaña, E., Perera-Pintado, A., Prats-Capote, A., Rodríguez-Tanty, C., and Altamirano-Bustamante, M. M. (2015) Drug Development in Conformational Diseases: A Novel Family of Chemical Chaperones That Bind and Stabilise Several Polymorphic Amyloid Structures. *PLoS One* 10 (9), No. e0135292.
(50) Chalifour, R. J., McLaughlin, R. W., Lavoie, L., Morissette, C., Tremblay, N., Boulé, M., Sarazin, P., Stéa, D., Lacombe, D., Tremblay, P., and Gervais, F. (2003) Stereoselective Interactions of Peptide Inhibitors with the β-Amyloid Peptide. *J. Biol. Chem.* 278 (37), 34874−34881.
(51) Rao, P. P. N., Mohamed, T., Teckwani, K., and Tin, G. (2015) Curcumin Binding to Beta Amyloid: A Computational Study. *Chem. Biol. Drug Des.* 86 (4), 813−820.
(52) Kumaraswamy, P., Sethuraman, S., and Krishnan, U. M. (2013) Mechanistic Insights of Curcumin Interactions with the Core-Recognition Motif of β-Amyloid Peptide. *J. Agric. Food Chem.* 61 (13), 3278−3285.
(53) Chen, D., Martin, Z. S., Soto, C., and Schein, C. H. (2009) Computational Selection of Inhibitors of Aβ Aggregation and Neuronal Toxicity. *Bioorg. Med. Chem.* 17 (14), 5189−5197.
(54) Tjernberg, L. O., Näslund, J., Lindqvist, F., Johansson, J., Karlström, A. R., Thyberg, J., Terenius, L., and Nordstedt, C. (1996) Arrest of -Amyloid Fibril Formation by a Pentapeptide Ligand. *J. Biol. Chem.* 271 (15), 8545−8548.
(55) Turner, J. P., Lutz-Rechtin, T., Moore, K. A., Rogers, L., Bhave, O., Moss, M. A., and Servoss, S. L. (2014) Rationally Designed Peptoids Modulate Aggregation of Amyloid-Beta 40. *ACS Chem. Neurosci.* 5 (7), 552−558.
(56) Törnquist, M., Michaels, T. C. T., Sanagavarapu, K., Yang, X., Meisl, G., Cohen, S. I. A., Knowles, T. P. J., and Linse, S. (2018) Secondary Nucleation in Amyloid Formation. *Chem. Commun.* 54 (63), 8667−8684.
(57) Van Lehn, R. C., and Alexander-Katz, A. (2013) Ligand-Mediated Short-Range Attraction Drives Aggregation of Charged Monolayer-Protected Gold Nanoparticles. *Langmuir* 29 (28), 8788−8798.
(58) Schwierz, N., Frost, C. V., Geissler, P. L., and Zacharias, M. (2016) Dynamics of Seeded Aβ40-Fibril Growth from Atomistic Molecular Dynamics Simulations: Kinetic Trapping and Reduced Water Mobility in the Locking Step. *J. Am. Chem. Soc.* 138 (2), 527−539.
(59) Lemkul, J. A., and Bevan, D. R. (2010) Assessing the Stability of Alzheimer's Amyloid Protofibrils Using Molecular Dynamics. *J. Phys. Chem. B* 114 (4), 1652−1660.
(60) Kahler, A., Sticht, H., and Horn, A. H. C. (2013) Conformational Stability of Fibrillar Amyloid-Beta Oligomers via Protofilament Pair Formation − A Systematic Computational Study. *PLoS One* 8 (7), No. e70521.
(61) Humphrey, W., Dalke, A., and Schulten, K. (1996) VMD: Visual Molecular Dynamics. *J. Mol. Graphics* 14 (1), 33−38.
(62) Drozdetskiy, A., Cole, C., Procter, J., and Barton, G. J. (2015) JPred4: A Protein Secondary Structure Prediction Server. *Nucleic Acids Res.* 43 (W1), W389−W394.
(63) Eswar, N., Webb, B., Marti-Renom, M. A., Madhusudhan, M. S., Eramian, D., Shen, M.-Y., Pieper, U., and Sali, A. (2006) Comparative Protein Structure Modeling Using Modeller. *Curr. Protoc. Bioinforma.* 15, 5.6.1.
(64) Van Lehn, R. C., and Alexander-Katz, A. (2013) Structure of Mixed-Monolayer-Protected Nanoparticles in Aqueous Salt Solution from Atomistic Molecular Dynamics Simulations. *J. Phys. Chem. C* 117 (39), 20104−20115.
(65) Schmid, N., Eichenberger, A. P., Choutko, A., Riniker, S., Winger, M., Mark, A. E., and van Gunsteren, W. F. (2011) Definition and Testing of the GROMOS Force-Field Versions 54A7 and 54B7. *Eur. Biophys. J.* 40 (7), 843−856.
(66) Poger, D., and Mark, A. E. (2012) Lipid Bilayers: The Effect of Force Field on Ordering and Dynamics. *J. Chem. Theory Comput.* 8 (11), 4807−4817.
(67) Berendsen, H. J. C., Postma, J. P. M., Gunsteren, W. F., and van Hermans, J. Interaction Models for Water in Relation to Protein Hydration. In *Intermolecular Forces*; Pullman, B., Ed.; The Jerusalem Symposia on Quantum Chemistry and Biochemistry; Springer: Netherlands, 1981; pp 331−342, DOI: 10.1007/978-94-015-7658-1_21.
(68) Darden, T., York, D., and Pedersen, L. (1993) Particle Mesh Ewald: An Nηlog(N) Method for Ewald Sums in Large Systems. *J. Chem. Phys.* 98 (12), 10089−10092.
(69) Essmann, U., Perera, L., Berkowitz, M. L., Darden, T., Lee, H., and Pedersen, L. G. (1995) A Smooth Particle Mesh Ewald Method. *J. Chem. Phys.* 103 (19), 8577−8593.
(70) Pronk, S., Páll, S., Schulz, R., Larsson, P., Bjelkmar, P., Apostolov, R., Shirts, M. R., Smith, J. C., Kasson, P. M., van der Spoel, D., Hess, B., and Lindahl, E. (2013) GROMACS 4.5: A High-Throughput and Highly Parallel Open Source Molecular Simulation Toolkit. *Bioinformatics* 29 (7), 845−854.
(71) Van Lehn, R. C., and Alexander-Katz, A. (2014) Free Energy Change for Insertion of Charged, Monolayer-Protected Nanoparticles into Lipid Bilayers. *Soft Matter* 10 (4), 648−658.
(72) Van Lehn, R. C., and Alexander-Katz, A. (2014) Fusion of Ligand-Coated Nanoparticles with Lipid Bilayers: Effect of Ligand Flexibility. *J. Phys. Chem. A* 118 (31), 5848−5856.
(73) Sharp, K. A., Nicholls, A., Fine, R. F., and Honig, B. (1991) Reconciling the Magnitude of the Microscopic and Macroscopic Hydrophobic Effects. *Science* 252 (5002), 106−109.
(74) Shrake, A., and Rupley, J. A. (1973) Environment and Exposure to Solvent of Protein Atoms. Lysozyme and Insulin. *J. Mol. Biol.* 79 (2), 351−371.

https://dx.doi.org/10.1021/acschemneuro.0c00497
ACS Chem. Neurosci. 2020, 11, 3153−3160